Anisotropy of the Reflected Radiation Field Over Melting Glacier Ice: Measurements in Landsat TM Bands 2 and 4

Wouter H. Knap* and Carleen H. Reijmer*

*I*n this article we analyze the anisotropy of the reflected radiation field over melting glacier ice using 118 ground-based radiance measurements in Landsat TM Bands 2 and 4. The measurements were carried out on the tongue of the Morteratschgletscher, Switzerland. On the basis of directional measurements several bidirectional reflectance distribution functions (BRDFs) were derived for dirty and clean glacier ice and for solar zenith angles between 46° and 60°. The anisotropic reflectance factor ranges between 0.70 and 1.60 for TM 2 and between 0.56 and 1.72 for TM 4. The BRDFs exhibit nadir darkening and maximum brightening near the forward limb. Dirty and wet ice reflect more anisotropically than clean ice. We give an example to illustrate the effect of anisotropic reflectance on the TM-derived albedo along a cross-section of the glacier. For solar zenith angles around 48° and in the nadir viewing direction we found differences of 0.05 (in TM 2) and 0.08 (in TM 4) between the albedo (a) and bidirectional reflectance (r). The differences prove to be more or less uniform for both clean ice and dirty ice. It is therefore suggested that one can convert r to a without having to classify the glacier surface. ©Elsevier Science Inc., 1998*

INTRODUCTION

Anisotropic reflectance of solar radiation on snow and ice surfaces complicates the retrieval of the surface albedo of glaciers from satellite measurements. Radiometers on board satellites record reflected radiation in one particular direction only, whereas measurements of radiation in all possible directions are needed to obtain a value of the upward irradiance. A correction for anisotropic behavior of the reflected radiation field should therefore be part of methods used to calculate the surface albedo from satellite measurements. Ground-based measurements of the directional dependency of the reflected radiation field over snow and ice are indispensable for an accurate derivation of the surface albedo of glaciers. Up to now such measurements have been carried out mainly over snow surfaces (e.g., Knowles Middleton and Mungall, 1952; Salomonson and Marlatt, 1968; Dirmhirn and Eaton, 1975; Kuhn, 1985; Steffen, 1987; Winther, 1993). Reflectance measurements over ice and snow were carried out, for example, by Hall et al. (1989) and Hall et al. (1990), but these measurements were confined to the nadir viewing angle only. Due to the lack of data it is not easy to make an accurate estimate of the surface albedo in ablation areas in particular or to assess the error involved if the reflected radiation field is assumed to be isotropic. This is an unfortunate situation because accurate estimates of satellite-derived glacier albedos could contribute to our understanding of the complex relationship between glacier behavior and climate change.

As a modest first step towards filling the existing gap in our knowledge of anisotropy of the reflected radiation field over glacier ice, we carried out reflectance measurements in the ablation zone of the Morteratschgletscher. This large valley glacier is situated in eastern Switzerland in the Bernina mountain range (Fig. 1). We decided to make the measurements there mainly because the glacier is accessible under almost all conditions. For the same reason the glacier was selected for various field studies concerning optical remote sensing and glaciometeorology. Numerous ground-based albedo measurements

* Institute for Marine and Atmospheric Research Utrecht, Utrecht University, Utrecht, The Netherlands

Address correspondence to Wouter H. Knap, Royal Netherlands Meteorological Institute, P.O. Box 201, 3730 AE De Bilt, The Netherlands. E-mail: knap@knmi.nl
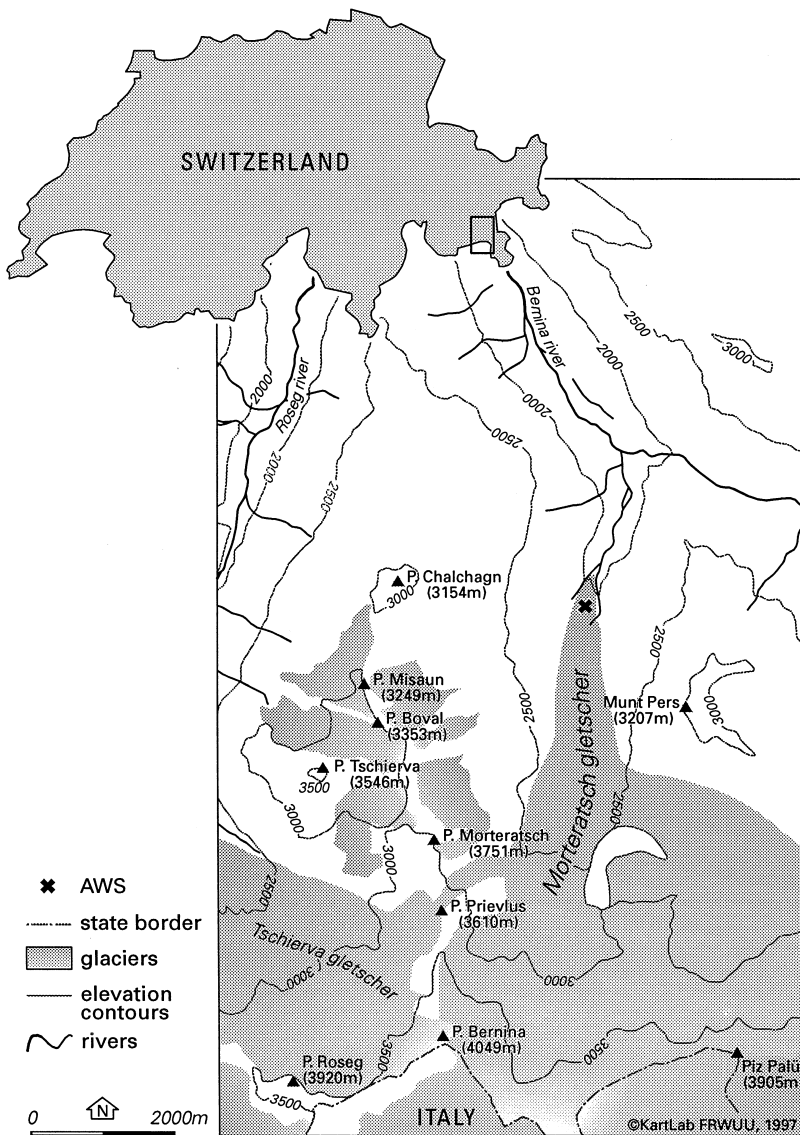
Figure 1. Map showing the Morteratschgletscher and the automatic weather station (AWS).

were carried out to derive a suitable expression for the derivation of the broadband albedo from narrowband albedos measured in Landsat Thematic Mapper (TM) Bands 2 and 4 (Knap et al., 1998a). In September 1996 an Automatic Weather Station (AWS) was installed on the tongue of the glacier (Fig. 1) to provide a multiannual data set of basic meteorological quantities (Oerlemans, 1997; Oerlemans and Knap, 1998).

Since Knap et al. (1998a) have recently derived an accurate narrowband-to-broadband conversion relationship on the basis of measurements in TM Bands 2 (visible radiation between 0.52 μm and 0.60 μm) and 4 (near-infrared radiation between 0.76 μm and 0.90 μm), the reflectance measurements presented here focus on anistropic behavior in the same wavelength bands. All measurements were made when the sky was cloudless, so that they are representative of typical conditions during which Landsat data, suitable for deriving the surface

albedo, are acquired. In order to relate the results presented here to the retrieval of the glacier albedo from TM data, a cloud-free Landsat image was used to derive the albedo along a cross-section of the tongue of the Morteratschgletscher. On the basis of the ground-based reflectance measurements we calculated the albedo with and without a correction for anisotropy.

DEFINITIONS AND FORMAL DESCRIPTION OF THE PROBLEM

Let I_i and I_r be the irradiance (W m^{-2}) incident on and reflected from the glacier surface. Both quantities refer to a plane that is parallel to the glacier surface. The surface albedo a is the ratio of reflected to incident irradiance:

$$a = \frac{I_r}{I_i}. \tag{1}$$

With the Sun at solar zenith angle θ_s and for viewing angles θ and φ (Fig. 2), the bidirectional reflectance is defined as follows:

$$r(\theta_s, \theta, \varphi) = \frac{R(\theta_s, \theta, \varphi)}{I_i/\pi}, \qquad (2)$$

in which $R(\theta_s, \theta, \varphi)$ is the reflected radiance (W m^{-2} sr^{-1}). The denominator is the diffuse radiance of a 100% reflective Lambertian surface (parallel to the glacier surface). If the radiation field over the glacier surface were isotropic, R would be independent of the view angles, so $a = r$. Deviation from isotropic reflection is quantified by the anisotropic reflectance factor $f(\theta_s, \theta, \varphi)$ which is related to the reflected radiance as follows:
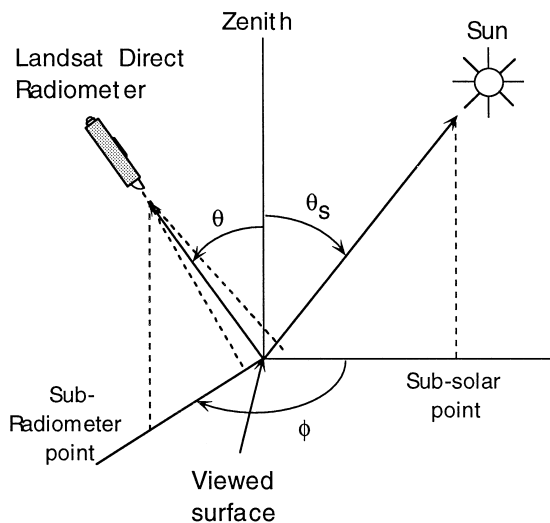
$$f(\theta_s, \theta, \varphi) = \frac{R(\theta_s, \theta, \varphi)}{I_r/\pi}. \qquad (3)$$

By combining Eqs. (1)–(3) it becomes clear that the anisotropic reflectance factor is in fact the ratio of the bidirectional reflectance to the albedo:

$$f(\theta_s, \theta, \varphi) = \frac{r(\theta_s, \theta, \varphi)}{a}. \qquad (4)$$

With respect to the retrieval of the surface albedo from satellite measurements, this equation states in a nutshell the problem induced by anisotropy of the reflected radiation field, namely, how to derive a from a satellite-derived measurement of $r(\theta_s, \theta, \varphi)$. It is clear that to derive a one needs to know distributions of $f(\theta_s, \theta, \varphi)$. For a fixed solar zenith angle, a complete distribution of f as a function of $\theta \in [0, \pi/2]$ and $\varphi \in [0, 2\pi]$ is called a bidirectional reflectance distribution function (abbreviated to BRDF).

INSTRUMENTS AND CALIBRATION

The set of instruments used during the field measurements on the Morteratschgletscher consisted of four pyranometers (radiometers with a hemispherical field of view) and two pyrheliometers (radiometers with narrow opening angle; in our case 5°), all constructed by Kipp & Zonen (Delft, The Netherlands). The pyranometers were built on the basis of a modification of the design of UV radiometers (type CUVB1), whereas the pyrheliometers were derived from the conventional pyrheliometer (type CH1) which is normally used for measurements of direct solar irradiance (Kipp & Zonen, 1996). The spectral response functions of the instruments were chosen close to the nominal Landsat 5 TM Bands 2 and 4. To indicate the relation between these instruments and the radiometers on board the Landsat satellite, the pyranometers were named Landsat Global Radiometer (LGR) and the pyrheliometers Landsat Direct Radiometer (LDR). Figure 3 shows the spectral response functions of LG(D)R and TM. As can be seen from this figure, the LG(D)R response functions are shifted by about 10 nm relative to the TM response functions. Note that the LG(D)R response functions are closer to the nominal TM values than are the actual TM response functions. Because albedo and anisotropy generally vary slowly with wavelength the wavelength shift causes only minor errors.

Before and after the field measurements the pyranometers were carefully calibrated against a 1000-W quartz-halogen lamp at the calibration laboratory of the Royal Netherlands Meteorological Institute (KNMI, De Bilt, The Netherlands). The pyrheliometers were calibrated in the field using a 99% Spectralon (a sintered polytetraflu-

Figure 2. Sun–surface–radiometer geometry. The view zenith angle and the relative view azimuth angle are denoted by θ and φ, respectively. The solar zenith angle is indicated by θ_s. The view azimuth angle φ is defined relative to the solar principal plane, that is, the sun is always at $\varphi = 0°$. Consequently, forward scattering corresponds to $\varphi = 180°$ and backscattering corresponds to $\varphi = 0°$.

Figure 3. Normalized relative spectral response functions of LG(D)R (ground-based radiometers) and TM (Thematic Mapper on board the Landsat satellite). The TM functions were adopted from Markham and Barker (1983). The nominal wavebands are 520–600 nm (visible) for TM 2 and 760–900 nm (near-infrared) for TM 4.
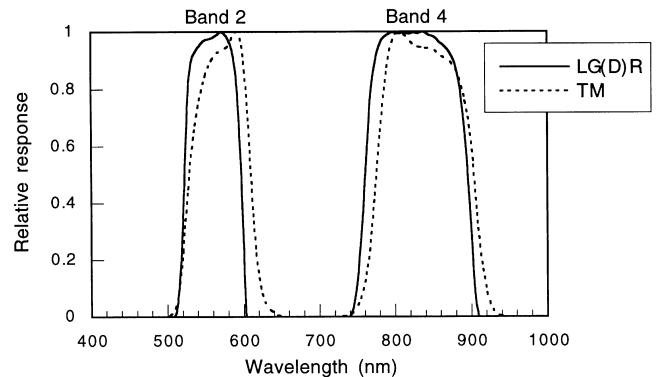
oroethylene-based material) reflectance panel. During periods with little or no cloud cover the LDRs were placed normal to the panel at a distance of about 75 cm. The global irradiance I_p (irradiance on the panel) in the two wavelength bands was measured with the LGRs. The pyrheliometer calibration factor K (in W m^{-2} sr^{-1} mV^{-1}) was obtained from Eq. (5):

$$r(0°/\theta_s) = \frac{KS}{I_p/\pi},\qquad (5)$$

where $r(0°/\theta_s)$ is the reflectance factor of the panel and S the voltage (in mV) across the LDR viewing the panel. For the designation of the reflectance factor we used the same notation as in Jackson et al. (1992). The part between brackets refers to a view angle of 0° and a source angle θ_s. Since the calibration was carried out in the field, the source angle was taken as the solar zenith angle. Unfortunately, the manufacturer of the panels (Labsphere) provides only a directional/hemispherical calibration $r(\theta/h)$ instead of the required directional/directional reflectance factor $r(0°/\theta_s)$. Since the panels are not perfectly diffuse reflectors, using $r(\theta/h)$ instead of $r(0°/\theta_s)$ introduces a certain error which is dependent on the source angle θ_s. Jackson et al. (1992) presented polynomials normalized to $r(0°/45°)$, which make it possible to estimate $r(0°/\theta_s)$ for each TM wavelength band. The directional/directional reflectance at 45° was estimated from the approximation $r(0°/45°)=1.015\times r(\theta/h)$, which was proposed by Hsia and Weidner (1981) on the basis of laboratory measurements. Jackson et al. (1992) correctly noted that the polynomials used to account for nonlambertian reflection of the Spectralon panels cannot give a highly accurate reflectance factor for any particular panel. The error involved in using the polynomials for estimating the reflectance of our panel is probably within 5%. The pyrheliometer calibration was carried out in June 1996 under cloudless conditions on the Morteratschgletscher (for $\theta_s \approx 30°$) and in October 1996 at a KNMI test site (for $\theta_s \approx 55°$). The calibration factors appeared to be highly reproducible ($<0.5\%$), so reductions in the sensitivity of the instruments can be ignored.

EXPERIMENT

Five series of radiance measurements were carried out near the AWS (see Figs. 1 and 13) during a few perfectly cloudless days in the second week of September 1996. The ice surfaces over which the measurements were made ranged between clean ice (broadband albedo 0.46) and dirty ice (broadband albedo 0.18). Further information about surface types and albedos observed on the Morteratschgletscher can be found in Knap et al. (1998a). In order to avoid effects of local surface topography, the measurements were carried out over a selection of relatively flat surfaces. Within the field of view of the radiometers, which was about 230 cm^2 for nadir measurements and a typical measurement height of 140 cm, there were

only small-scale irregularities (i.e., typical size≪field of view). Due to the time of year, measurements for small solar zenith angles could not be made, and the range of the solar zenith angle covered was moderate (at most between 46° and 60°).

The BRDF measurements were carried out as follows. Two LDRs (acquiring data in TM Bands 2 and 4) and an inclinometer were fixed to a small aluminium frame. A thin (0.4 mm diameter) synthetic fiber was stretched from the instruments to a screw that was driven into the ice. The instruments were pointed manually towards the surface by stretching the fiber tightly. The view zenith and azimuth angles were adjusted by means of the inclinometer and a compass. The uncertainty in θ and φ is estimated to be less than 3° and 10°, respectively, which is acceptable in view of the angular resolution of the measurements (see also Table 1). Since the view geometry was established relative to the horizontal plane the horizontal polar coordinates were transformed to surface-parallel polar coordinates (two rotations). All our results will be presented in these coordinates. In order to reduce random errors (arising from, i.e., variations in θ), we took, for each pair of view angles (θ, φ) and for each spectral band, six samples. The data were stored in a Campbell CR 10 datalogger. The time needed to acquire data for one point of the BRDF was about 1 min. One series of measurements took roughly between 1/2 h and 1 h, depending on the angular resolution applied. In order to keep the Sun at $\varphi=0°$ (so as to achieve the correct relative azimuth angle), the azimuthal direction of the Sun was reestablished after the measurements in the θ direction were made. Each series of measurements was ended with a measurement of the incident and reflected irradiance.

METHOD OF CONSTRUCTING BRDFs

During each series of measurements, variation in the solar zenith angle (see Table 1) caused variation in the irradiance on the glacier surface. Since the irradiance was not measured continuously (only once; at the end of each series of measurements), we calculated the relative variation in the irradiance on the basis of the following simple model, which is based on partitioning of the irradiance into a direct and a diffuse part:

$$I_i(t) = I_0\,\mu(t) + D.\qquad (6)$$

Here I_0 is the direct irradiance on a surface perpendicular to the solar beam and $\mu(t) = \cos \theta_s(t)$ at time t. D is the diffuse irradiance. The contribution of D to the total irradiance was estimated using a radiative transfer model based on the 24-band radiation scheme described by Slingo and Schrecker (1982).

Equation (6) should be applied only under the condition that changes in the atmospheric conditions are small. In order to obtain an impression of these conditions during the reflectance measurements, we analyzed meteorological data recorded at the AWS. The data sug-

Table 1. Some Details about the Radiance Measurements Carried Out for the Construction of BRDFs of Glacier Ice[a]

Series	n	θ_s (Relative)	Ice Surface	Slope	Albedo	View Resolution	
						$\Delta\theta$	$\Delta\varphi$
1	14	52–55°	Clean, white	6°	0.46	20°	90°
2	24	47–48°	Clean, some water	6°	0.38	20°	45°
3	17	58–60°	Moderately clean	6°	0.35	15°	90°
4	33	48–53°	Clean, some water	4°	0.40	10°	45°
5	30	46–49°	Dirty wet	4°	0.18	10°	45°

[a] The number of measurements per series is indicated by *n*. For each series the variation in the solar zenith angle (θ_s) relative to the glacier surface is given. The cloud amount was always 0/8. A characterization of the glacier surface and the (broadband) albedo are given. The resolution in the view zenith angle θ and the view azimuth angle φ is given in the last two columns.

gested uniform conditions characterized by a wind regime dominated by katabatic flow (see also Oerlemans, 1997). Furthermore, we verified Eq. (6) by using the time series of global radiation measured at the AWS. The analysis (not presented here) showed that during the prevailing conditions accurate results (error<2%) could be obtained if periods of 1/2 h to 1 h were considered.

Although the number of radiance measurements per series is considerable (Table 1), there are not enough measurements to construct complete BRDFs on the basis of standard interpolation and extrapolation techniques. Therefore, the following parameterized form of the anisotropic reflectance factor was used:

$$f = a_0 + a_1 x + a_2 x^2 + a_3 y + a_4 y^2 + a_5 \mu + a_6 y\mu, \quad (7a)$$

where

$$x = \sin\theta \sin\varphi \quad (7b)$$

and

$$y = \sin\theta \cos\varphi \quad (7c)$$

and

$$\mu = \cos\theta_s. \quad (7d)$$

Lindsay and Rothrock (1994) used this form to parameterize anisotropic reflectance factors derived from Nimbus-7 Earth Radiation Budget (ERB) data (Taylor and Stowe, 1984). The parameterization gave a smooth representation of the BRDF of various scene types such as ocean, land, snow, desert, and cloud. We anticipated that the parameterization would also be suitable for glacier ice. Due to the lack of measurements for different solar zenith angles, the dependency on μ was omitted ($a_5 = a_6 = 0$). Furthermore, the parameterization was forced to be azimuthally symmetric ($a_1 = 0$). On the basis of multiple linear regression, values of the coefficients a_i were calculated for each of the two wavelength bands and for each of the five surface types.

The calculated parameterizations were verified using the normalization condition given by Eq. (8):

$$\pi^{-1} \int_0^{2\pi} \int_0^{\pi/2} f(\theta, \varphi) \sin\theta \cos\theta \, d\theta \, d\varphi = 1. \quad (8)$$

It turned out that the parameterizations did not satisfy

this condition: averaged over 10 BRDFs, the integral equalled 1.13π instead of π. There are two possible causes: a) The parameterization is not capable of giving an accurate representation of the measurements, or b) the measurements of the anisotropic reflectance factors suffer from a systematic error. In order to examine cause a), the residuals of the parameterization were correlated with the view angles. Since no correlation was found, there is no particular area in the view domain that is badly represented by the parameterization. Probably the limb only is not well modeled because no measurements were (and can be) carried out at the very edge of the view domain. In order to test the sensitivity of the integral to errors at the limb, the integration was cut off at $\theta = 80°$ (i.e., $f = 0$ for $\theta > 80°$). The effect proved to be much smaller than 13%. Altogether, it seems improbable that the parameterization caused the departure from the normalization condition. More probably the cause of the deviation was a systematic error in the anisotropic reflectance factors. There are two sources of uncertainty which may have contributed to errors in the anisotropic reflectance factor. First and foremost the ground area sensed by the down-facing pyranometer is much larger than the area sensed by the pyrheliometers. An ideal measurement of the upward irradiance would have covered only the area sensed by the pyrheliometer. According to measurements not presented here, small scale variations in the reflectance can be substantial, so a significant error in the upward irradiance is conceivable. Second, there is uncertainty in the pyrheliometer calibration (see the third section). Most probably the overall uncertainty in the anisotropic reflectance factor is large enough to explain the departure from the normalization condition. In order to account for systematic errors, the anisotropic reflectance factors of each series were systematically adjusted so that they integrated to π. The magnitude of the correction factors ranged between 3% and 19%.

RESULTS

The coefficients a_i and some statistics are summarized in Table 2. For all fits there is statistically significant correlation between parameterized and measured anisotropic

Table 2. Parameterized BRDFs Based on *n* Measurements of *f* [Eqs. (3) and (7)][a]

Series	TM	n	a_0	a_2	a_3	a_4	r^2	σ_{res}
1	2	14	0.934	0.005	−0.103	0.261	0.63	0.089
1	4	14	0.904	0.060	−0.201	0.325	0.83	0.072
2	2	24	0.923	0.125	−0.148	0.182	0.82	0.047
2	4	24	0.857	0.222	−0.218	0.350	0.88	0.062
3	2	17	0.862	0.234	−0.329	0.317	0.93	0.063
3	4	17	0.760	0.387	−0.299	0.573	0.88	0.010
4	2	33	0.900	0.138	−0.089	0.262	0.84	0.044
4	4	33	0.810	0.251	−0.243	0.510	0.90	0.072
5	2	30	0.804	0.359	−0.237	0.426	0.91	0.067
5	4	30	0.621	0.701	−0.141	0.815	0.92	0.092

[a] $a_1 \equiv a_5 \equiv a_6 \equiv 0$ (see text). The correlation coefficient and the standard deviation of the residuals are given by r^2 and σ_{res}, respectively.

reflectance factors. Considering all data points (118), it was found that the residual standard deviation is 0.05 for TM 2 and 0.07 for TM 4. In near-nadir direction (say $\theta < 20°$) the values are slightly smaller: 0.04 and 0.06, respectively. The quality of the fit is visualized in Figure 4, where the parameterized factors are plotted against the measured factors. The main line of the measurements is represented quite well. In order to find out whether improvement is possible other models such as $f = a\theta^2 + b\theta \cos \varphi$ (Walthall et al., 1985) were tested, but Eq. (7a–d) gave the best results.

The five BRDFs are presented as polar diagrams in Figures 5–9. The radial coordinate represents the view zenith angle θ and the azimuthal coordinate represents the relative Sun–radiometer azimuth φ (see Fig. 2). The BRDFs will now be described in turn.

Figure 5 shows the BRDF of clean ice for solar zenith angles ranging from 52° to 55°. The ice contained relatively few impurities and appeared very bright (al-

most white) to the human eye, which is not surprising considering the high albedo in TM 2 (0.62). Little meltwater was present at the surface. In TM 2 the BRDF is rather flat. In the near-nadir direction (say $\theta < 10°$) the pattern suggests values around 0.95. In other words, a single radiance measurement in this direction would underestimate the upward flux and albedo by 5% if isotropy were assumed. In general the reflectance increases as the ice surface is viewed at larger zenith angles (limb brightening), but in the sideward direction ($\varphi = 90°$) the pattern is nearly flat with values close to 0.95. Forward scattering ($\varphi = 180°$) is more pronounced than backscattering ($\varphi = 0°$).

The shape of the BRDF in TM 4 (lower part of Fig. 5) is similar to the BRDF in TM 2, but forward scattering is more pronounced in the near-infrared. This fea-

Figure 4. Parameterized anisotropic reflectance factors on the basis of Eq. (7) versus measured anisotropic reflectance factors in TM Bands 2 and 4.

Figure 5. BRDF for clean dry glacier ice and for solar zenith angles between 52° and 55°. The narrowband albedos are 0.62 (TM 2) and 0.53 (TM 4). The broadband albedo is 0.46.
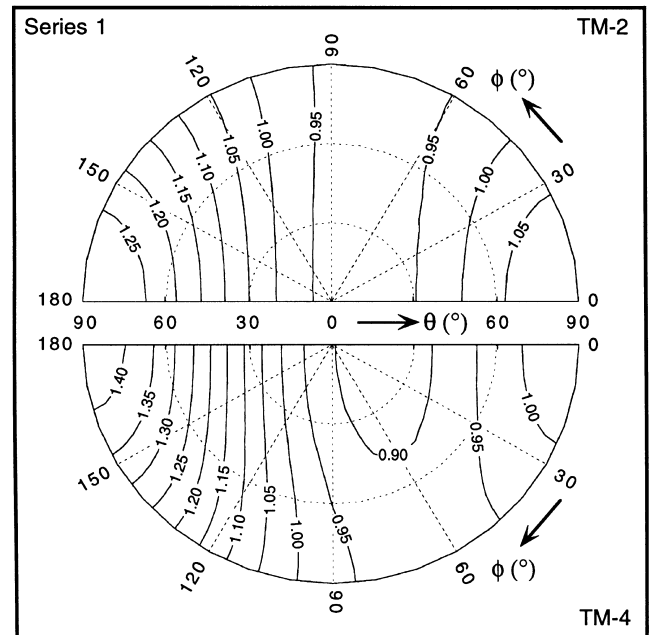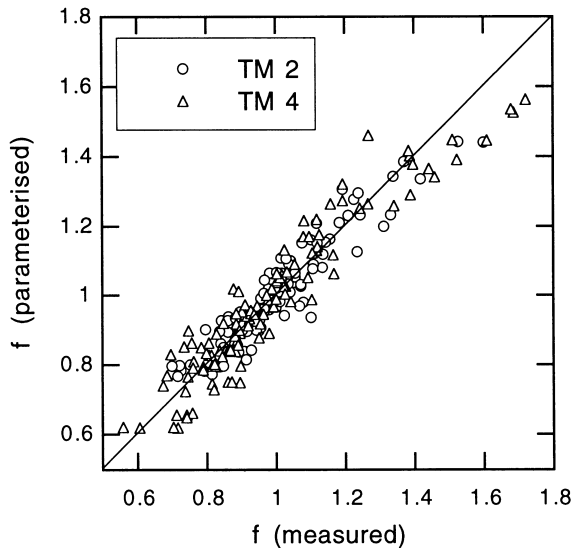
ture is in agreement with model calculations of the al-
bedo of snow (Wiscombe and Warren, 1980). The basic
reason is that ice is more absorptive in the near-infrared
than in the visible, so that the number of scattering
events is suppressed at the longer wavelengths. Broadly
speaking, the BRDF "remembers" more of the extreme
asymmetry of the scattering between photons and *indi-
vidual* grains if the wavelength is longer [asymmetry re-
fers to the fact that scattering within a few degrees of
the forward direction is much more probable than scat-
tering in other directions (Warren, 1982)]. This effect is
greatly enhanced by the fact that the single-particle for-
ward scattering increases for longer wavelengths. Going
back to the lower part of Figure 5, we see that the pro-
nounced brightening at the forward limb is compensated
by darkening in the near-nadir area. In this direction the
near-infrared BRDF suggests values around 0.90.

The second series of radiance measurements was
carried out over relatively clean ice with some meltwater
at the surface. Due to the meltwater and the presence
of a little fine-grained material, the broadband albedo is
significantly lower than the broadband albedo of the
clean ice described previously (0.38 compared to 0.46).
The reduction is due primarily to a decrease in the al-
bedo in the near-infrared. The BRDF of this type of ice
for solar zenith angles between 47° and 48° is shown in
Figure 6. The pattern is similar to the pattern of clean
ice (Fig. 5), but sideward scattering ($\varphi=90°$) is more pro-
nounced. Again, brightening at the forward limb and
near-nadir darkening are more pronounced in TM 4 than

Figure 7. BRDF for moderately clean glacier ice with some
water at the surface and for solar zenith angles between 58°
and 60°. The narrowband albedos are 0.59 (TM 2) and 0.44
(TM 4). The broadband albedo is 0.35.

in TM 2. In the near-nadir direction the assumption of
isotropy would underestimate a_2 by 5–10% and a_4 by
10–15%.

The physical state of the third surface was similar to
that of the second surface. However, the solar zenith
angle was about 10° larger, so that anisotropy should be
more pronounced. Figure 7 shows that this is indeed
true. Brightening towards the forward limb is relatively
strong with anisotropic reflectance factors up to about
1.6. Near-nadir darkening is prominent as can be seen
from the values in TM 2 (0.80-0.90) and in TM 4
(around 0.75).

The surface and the range of solar zenith angles for
series 4 is more or less the same as for series 2. The
BRDFs of both series are therefore to a large extent the
same (Fig. 6 and Fig. 8). The only difference is that se-
ries 4 reveals brightening at the entire limb, whereas the
BRDF of series 2 shows some darkening in the backward
direction ($\varphi=0°$).

The last series of radiance measurements was carried
out over dirty and wet glacier ice. Fine-grained material
and water were evenly distributed over a relatively smooth
ice surface. The broadband albedo was very low (0.18).
Figure 9 shows the BRDF of this surface for solar zenith
angles ranging between 46° and 49°. Clearly the large ab-
sorption causes the BRDF to be strongly anisotropic. Due
to the darkness of the surface and to the pronounced con-
trast between near-nadir and limb reflectances, the aniso-
tropic character of the radiation field could be clearly ob-
served by the human eye. The BRDFs suggest strong

Figure 6. BRDF for clean glacier ice with some water at
the surface and for solar zenith angles between 47° and 48°.
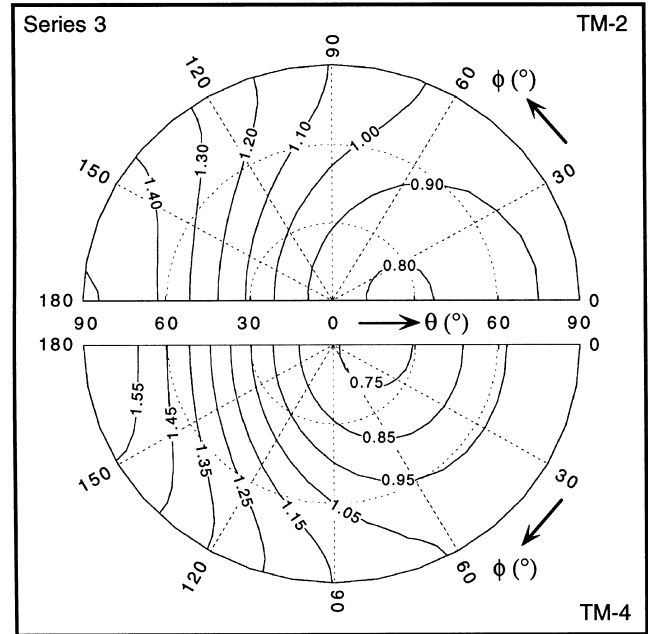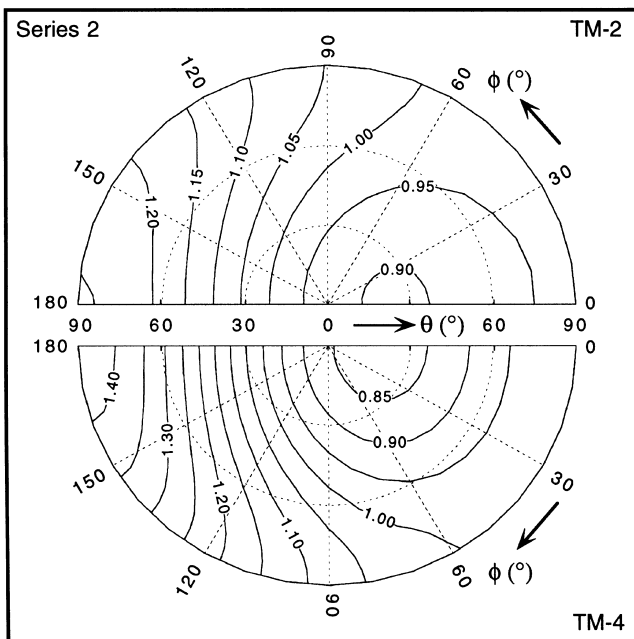The narrowband albedos are 0.58 (TM 2) and 0.45 (TM 4).
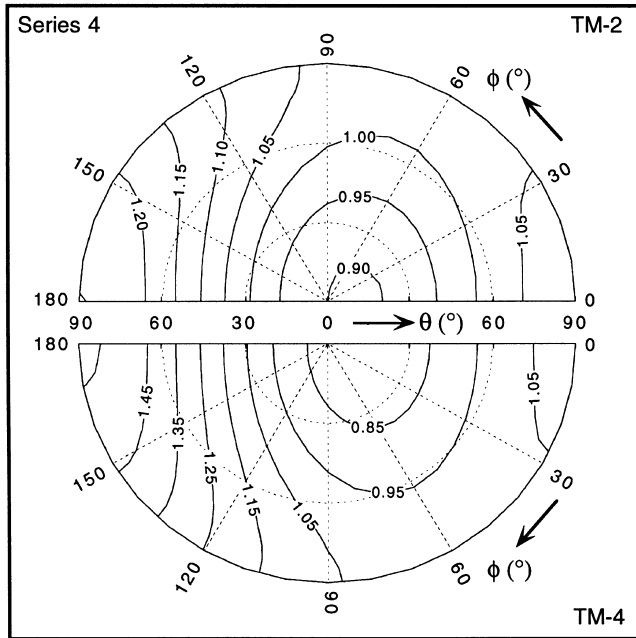The broadband albedo is 0.38.

Figure 8. BRDF for clean glacier ice with some water at the surface and for solar zenith angles between 48° and 53°. The narrowband albedos are 0.59 (TM 2) and 0.46 (TM 4). The broadband albedo is 0.40.
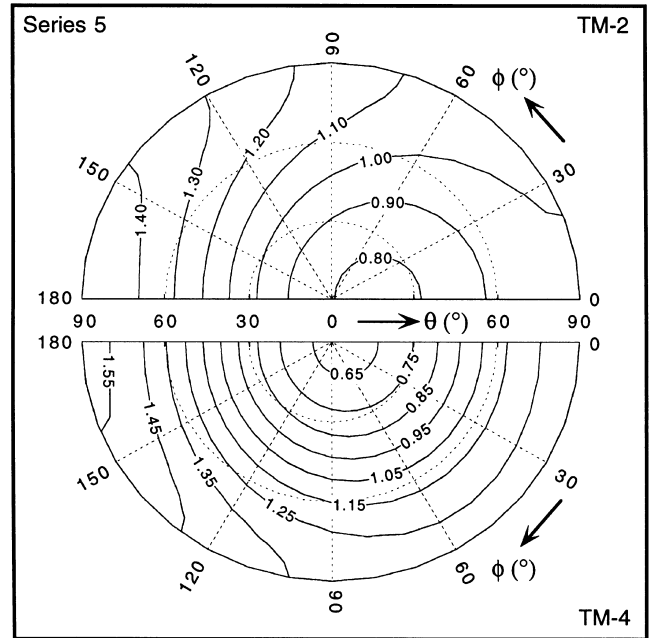

Figure 9. BRDF for dirty glacier ice with some water at the surface and for solar zenith angles between 46° and 49°. The narrowband albedos are 0.25 (TM 2) and 0.20 (TM 4). The broadband albedo is 0.18.

darkening in the near-nadir direction. In TM 2 the isotropic assumption underestimates the upward flux by about 20%. The error may be as much as 35% in TM 4.

COMPARISON WITH PREVIOUS MEASUREMENTS

Unfortunately, our measurements cannot be compared in detail with results presented in previous literature because, as far as we know, measurements in ablation areas of valley glaciers have not been carried out before. Nevertheless, some data on anisotropy over superimposed ice (Winther, 1994) and snow and water (Suttles et al., 1988) are available, and so a rough comparison is possible.

Winther (1994) presented spectral measurements of the bidirectional reflectance (r) of superimposed ice on a glacier in Dronning Maud Land (Antarctica). The reflectances measured in Antarctica should be compared with measurements carried out over the cleanest ice that we found on the Morteratschgletscher (see the BRDF of Fig. 5). The measurements in Antarctica were carried out exclusively in the forward direction ($\varphi=180°$) with the Sun at $\theta_s=59°$ (compare this with $\theta_s=52$–$55°$ for series 1). Unfortunately, the albedo (a) was not measured, so that absolute values of the anisotropic reflectance factor (f) could not be obtained from these data. Therefore, we normalized all measurements to the nadir (i.e., $\theta=0°$) reflectance. Figure 10 shows both the measurements in Antarctica and Switzerland. The figure suggests that, at least in the present case, anisotropy over superimposed ice is more pronounced than over clean glacier ice. This

may be due to differences in the physical composition of the two surfaces, although the difference in the solar zenith angle may also have played a role. With respect to the wavelength dependency of the anisotropic reflectance factor, the measurements carried out over clean glacier ice are consistent with those made over superimposed ice. Namely, both measurements revealed that anisotropy in the near-infrared (TM 4) is stronger than in the visible (TM 2).

Figure 10. Anisotropic reflectance factors for $\varphi=180°$ and $\theta_s=59°$ derived from radiance measurements over superimposed ice in Dronning Maud Land, Antarctica [measurements adopted from Winther (1994) and presented as solid curves]. The dotted curves refer to parameterized anisotropic reflectance factors of clean glacier ice derived from measurements on the Morteratschgletscher for $\theta_s=52$–$55°$. All reflectance factors were normalized to the nadir value ($\theta=0°$).
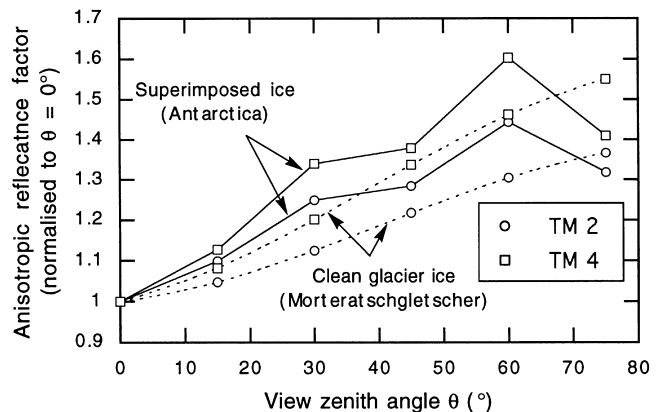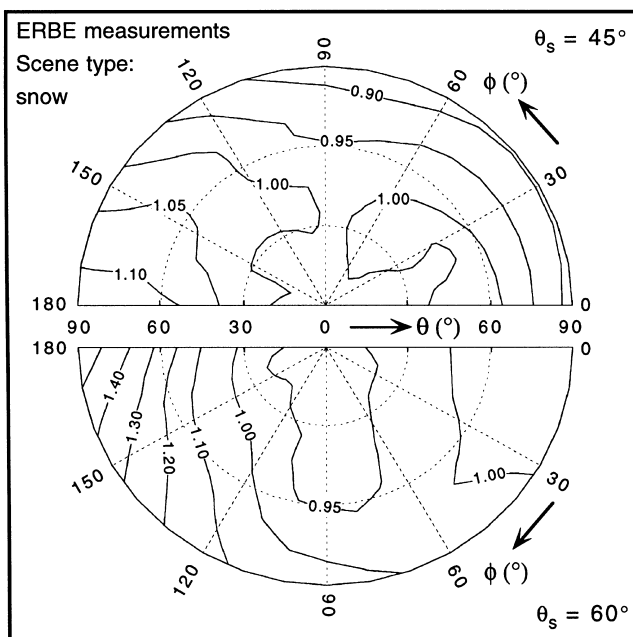
Suttles et al. (1988) compiled an extensive data set of BRDFs on the basis of spaceborne radiance measurements carried out by the Nimbus 7 Earth Radiation Budget (ERB) instrument (Jacobowitz et al., 1984). Several optical telescopes within this scanning instrument supplied data for deriving broadband shortwave (0.2–4 μm) BRDFs over a variety of scenes such as ocean, land, snow, desert, and cloud. The ground resolution of the ERB instrument is about 90 km×90 km at nadir and increases to about 250 km×250 km at the maximum scan angle. Since ablation areas of glaciers are usually much smaller than this resolution, it is not surprising that there is no scene type "glacier ice" available from the ERB data set. Of all scene types presented in the data set the types "snow" and "ocean" are probably the most closely related to glacier ice, although it is obvious that a comparison on the basis of these types is less ideal than the comparison described above.

Figure 11 shows the ERB-derived BRDF of snow for $\theta_s=45°$ and $\theta_s=60°$. For $\theta_s=45°$ the pattern is extremely flat and for $\theta<60°$ the anisotropic reflectance factor is generally close to 1. Only near the limb can some brightening and darkening be observed. None of the BRDFs derived from measurements on the Morteratschgletscher reveals such a flat and near-isotropic reflectance pattern. However, the ERB-derived BRDF of snow for $\theta_s=60°$ is quite similar to the TM-4 BRDFs of clean glacier ice (compare Figs. 5 and 8 with Fig. 11). In both cases the BRDF is characterized by limb brightening and near-nadir darkening. There is even broad

agreement on the values of the anisotropic reflectance factor.

Figure 12 shows the ERB-derived BRDF of ocean again for $\theta_s=45°$ and $\theta_s=60°$. The pattern is highly anisotropic and Sun glint (resulting from specular reflection) can be observed near $\theta=\theta_s$ for $\varphi=180°$. None of the BRDFs of glacier ice is as anisotropic as the pattern of water. Only the BRDF of dirty and wet ice (Fig. 9) shows some resemblance with the pattern of water for $\theta_s=45°$. Near-nadir darkening occurs rather strongly in both BRDFs. Most probably the agreement is due to the presence of melt water on the glacier surface.

IMPLICATIONS FOR LANDSAT 5 TM DERIVED SURFACE ALBEDO

On the basis of a realistic example we will now demonstrate that it may be essential to include a correction for anisotropic reflection in methods of retrieving the surface albedo from radiances measured by the TM radiometer. To make it possible to examine the consequence of assuming an isotropic reflected radiation field ($a=r$; see the second section), we derived both the surface albedo a and the bidirectional surface reflectance r along a cross section of the Morteratschgletscher (Fig. 13). Details of how these quantities were obtained will be given next.

Albedo along the Cross-Section

Besides the BRDF measurements presented above, numerous measurements of the broadband albedo a and the narrowband albedos a_2 (TM 2) and a_4 (TM 4) were

Figure 11. BRDF of snow derived from ERB Experiment measurements (Suttles et al., 1988). In the upper panel the solar zenith angle is 45° whereas in the lower panel the solar zenith angle is 60°.

Figure 12. BRDF of ocean derived from ERBE measurements (Suttles et al., 1988). In the upper panel the solar zenith angle is 45° whereas in the lower panel the solar zenith angle is 60°.
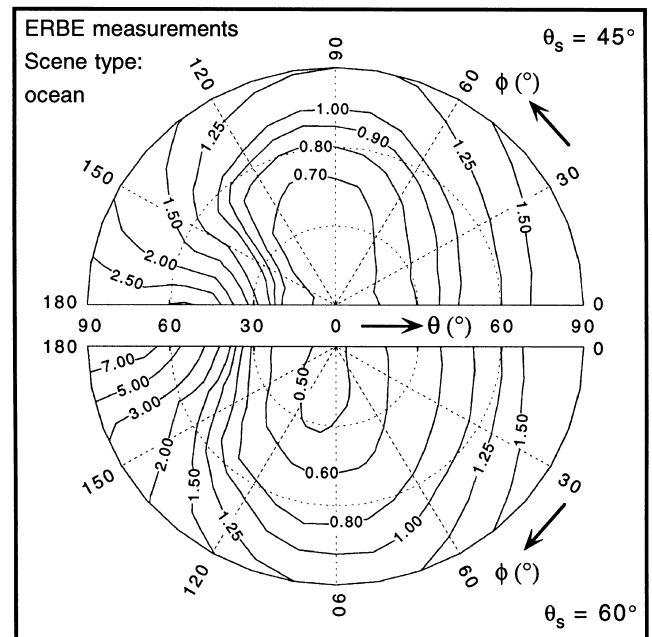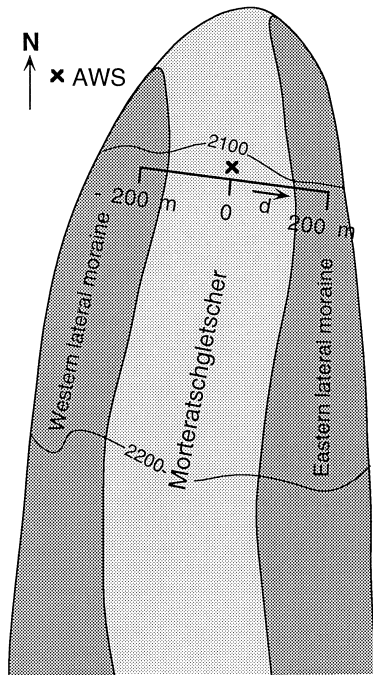
Figure 13. Map of the tongue of the Morteratschgletscher showing the location of the cross-section along which the albedo was derived (see Figs. 14 and 15).

Figure 14. Satellite-derived surface albedo along a cross-section taken on the tongue of the Morteratschgletscher on 26 July 1996. The position of the cross section is indicated in Figure 13. For details of the retrieval method (which includes an atmospheric correction) the reader is referred to Knap et al. (1998b).

carried out in order to derive a relationship for narrowband to broadband conversion of glacier albedos (Knap et al., 1998a). The measurements were carried out at random positions in the immediate surroundings of the cross section presented in Figure 13. Highest albedo values were measured in the middle of the glacier where the concentration of supraglacial material is relatively low. Towards the sides of the glacier, more material occurred at the surface and the albedo was frequently lower. According to the surface albedo derived from a cloud-free Landsat 5 TM image (acquired on 26 July 1996) the distribution of the albedo along the cross section can be accurately described by a Gaussian function (Fig. 14). In order to obtain an albedo distribution representative of the situation during the second week of September, the top and asymptotic values of the Gaussian function were forced to the ground-based albedo values measured in the middle and near the sides of the glacier, respectively. The resulting Gaussian function gives an idealized distribution of the albedo, which is most probably close to reality.

Bidirectional Reflectance along the Cross-Section

Since the physical composition of the surface varies strongly along the cross section, it is obvious that the BRDF, needed to calculate the bidirectional reflectance out of the albedo, is not uniform. The BRDF measure-
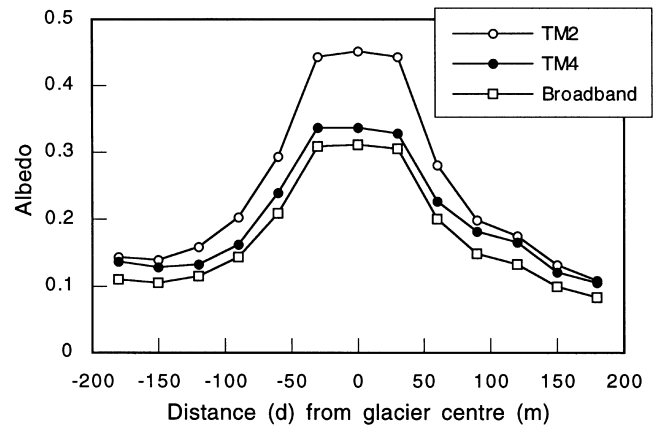
ments presented above suggested that the degree of anisotropy increases with decreasing albedo. In order to take this effect into account, it is assumed (as a first guess!) that the anisotropic reflectance factor is a linear function of the albedo. Only BRDF 2 (Fig. 6) and BRDF 5 (Fig. 9) are suitable for interpolation because these patterns represent extreme cases of anisotropy and are valid for about the same range of solar zenith angles ($\theta_s=46$–$49°$). The two BRDFs were derived from measurements at $d=0$ and $d=-80$ m, respectively (see Fig. 13). The analysis will therefore be restricted to $|d|\leqslant80$ m. Furthermore, we will confine our investigation to a situation in which the glacier surface is viewed in the nadir direction (i.e., $\theta=0°$).

On the basis of the relationship between the albedo and the bidirectional reflectance ($r=f\times a$) and by linearly interpolating the nadir anisotropic reflectance factors, we calculated narrowband bidirectional reflectances along the cross section. Broadband reflectances were calculated using an empirical relationship presented in Knap et al. (1998a).

Discussion

The narrowband and broadband albedo and the bidirectional reflectance along the cross section are presented in Figure 15. The lateral coordinate is indicated by d, with $d=0$ in the middle of the glacier. Numerical results at $d=0$ and $|d|=80$ m are summarized in Table 3. The values of r are given with errors which reflect uncertainty introduced by using the parameterized form of the anisotropic reflectance factor [Eq. (7a–d)]. As was described before, anisotropy is most pronounced in the near-infrared. In the middle of the glacier $a_4=0.48$, whereas r_4 is only 0.41 ± 0.03. This implies that the isotropic assumption causes an overestimation of 13% of
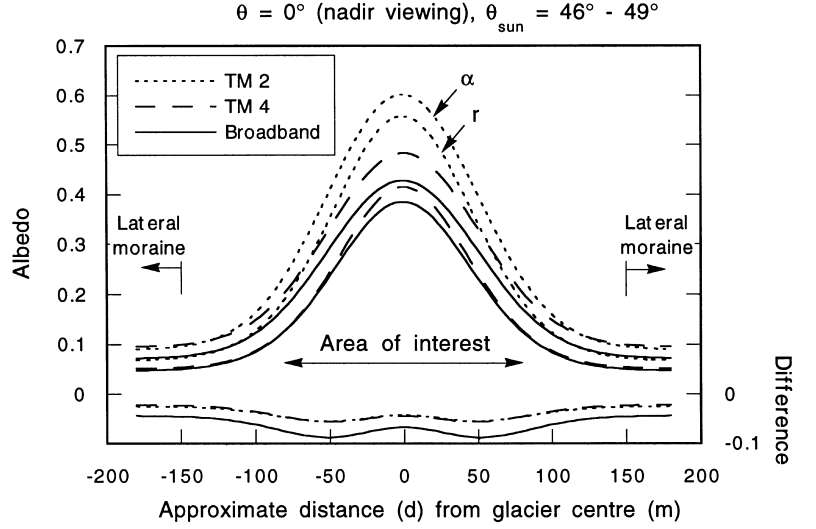
θ = 0° (nadir viewing), θ_sun = 46° - 49°

Figure 15. Gaussian-shaped albedo cross-sections of the Morteratschgletscher for September 1996. Of each pair of lines the upper one is the albedo (*a*) and the lower one the bidirectional reflectance (*r*). The lowest curves represent the difference between the bidirectional reflectance and albedo for each wavelength band.

the absorbed flux in TM 4. In TM 2, the absorbed flux is overestimated by 11%. The broadband albedo is lower than both the narrowband albedos so that the error in the absorbed broadband flux is smaller: 7% at $d=0$. At $|d|=80$ m, the anisotropic character of reflectance is much stronger than in the middle of the glacier. On the other hand, the albedo is significantly lower, so that the error of 6% in the broadband absorbed flux is about the same as in the middle of the glacier.

The results presented in Table 3 and Figure 15 suggest that the difference between albedo and bidirectional reflectance $(a-r)$ is more or less uniform for both high albedo values (weak anisotropy) and low albedo values (strong anisotropy). In consequence, simple systematic corrections of the form "$a=r+\text{constant}$" would make it possible to calculate accurate albedo values from bidirectional reflectances without having to classify the glacier surface. It is obvious that this would be of great benefit for remote sensing applications.

CONCLUDING REMARKS

Considering all measurements, it was found that the anisotropic reflectance factor ranged between 0.70 and 1.60 in TM 2 and between 0.56 and 1.72 in TM 2. We therefore conclude that the reflected radiation field over glacier ice could be strongly anisotropic. Therefore, significant errors in satellite-derived albedos may arise from

the assumption that the radiation field is isotropic. For example, it was found that the difference between the albedo (*a*) and the bidirectional reflectance (*r*) is +0.05 for TM 2 and +0.08 for TM 4. These numbers were derived for solar zenith angles between 46° and 49° and for nadir viewing direction. Striking is that the differences proved to be more or less uniform for both clean ice (high albedo and weakly anisotropic) and for dirty, wet ice (low albedo and strongly anisotropic). It is obvious that this is a favorable result for remote sensing applications because it may imply that a conversion from bidirectional reflectance to albedo is possible without a classification of the glacier surface. We therefore propose to seek empirical expressions of the form:

$$a_2 = r_2(\theta_s, \theta, \varphi) + c_2(\theta_s, \theta, \varphi),$$
$$a_4 = r_4(\theta_s, \theta, \varphi) + c_4(\theta_s, \theta, \varphi). \qquad (9)$$

Here c_2 and c_4 are anisotropic correction factors for TM Bands 2 and 4, respectively, which depend only on the solar zenith angle θ_s and the viewing angles θ and φ and not on the physical composition of the ice surface. This approach contrasts with conventional corrections which are based on surface-dependent relationships of the form $a=r(\theta_s, \theta, \varphi)/f(\theta_s, \theta, \varphi)$ [see Eq. (4)]. It is clear that the data set presented here is too limited to thoroughly test the validity of Eq. (9). Additional radiance measurements under different solar zenith angles and over different

Table 3. Albedo (*a*), Bidirectional Nadir Reflectance (*r*), and Error in the Absorbed Flux (ΔQ_{abs}) if Isotropic Reflectance Assumed[a]

Site	TM 2 (Visible)			TM 4 (Near-Infrared)			Broadband		
	a	*r*	ΔQ_{abs}	*a*	*r*	ΔQ_{abs}	*a*	*r*	ΔQ_{abs}
$d=0$	0.60	0.56±0.02	11%	0.48	0.41±0.03	13%	0.43	0.38±0.03	7%
$|d|=80$	0.24	0.19±0.01	6%	0.20	0.13±0.01	10%	0.17	0.13±0.01	6%

[a] The values of *r* were calculated on the basis of BRDF 2 (measured at $d=0$) and BRDF 5 (measured at $d=80$ m). These BRDFs are valid for solar zenith angles between 46° and 49°. The errors in *r* reflect uncertainty caused by the parameterization [Eq. (7)].

types of glacier ice are therefore needed to extend the BRDF data set presented here.

REFERENCES

Dirmhirn, I., and Eaton, F. D. (1975), Some characteristics of the albedo of snow. *J. Appl. Meteorol.* 14:375–379.

Hall, D. K., Chang, A. T. C., Foster, J. L., Benson, C. S., and Kovalick, W. M. (1989), Comparison of in situ and Landsat derived reflectance of Alaskan glaciers. *Remote Sens. Environ.* 28:23–31.

Hall, D. K., Bindschadler, R. A., Foster, J. L., Chang, A. T. C., and Siddalingaiah, H. (1990), Comparison of in situ and TM-derived reflectances of Forbindels Glacier, Greenland. *Int. J. Remote Sens.* 11(3):493–504.

Hsia, J. J., and Weidner, V. R. (1981), NBS 45°/normal reflectometer for absolute reflectance factors. *Metrologia* 17:97–102.

Jackson, R. D., Clarke, T. R. C., and Moran, M. S. (1992), Bidirectional calibration results for 11 spectralon and 16 BaSO$_4$ reference reflectance panels. *Remote Sens. Environ.* 40:231–239.

Jacobowitz, H., Soule, H. V., Kyle, H. L., House, F. B., and NIMBUS 7 ERB Experiment Team (1984), The Earth Radiation Budget (ERB) Experiment: an overview. *J. Geophys. Res.* 89(D4):5021–5038.

Kipp & Zonen (1996), Radiation sensors including special sensor design and calibration services, Documentation, Kipp & Zonen, Delft, The Netherlands.

Knap, W. H., Reijmer, C. H., and Oerlemans, J. (1998a), Narrowband to broadband conversion of Landsat-TM glacier albedos. *Int. J. Remote Sens.*, in press.

Knap, W. H., Brock, B. W., Oerlemans, J., and Willis, I. C. (1998b), Comparison of Landsat-TM derived and ground-based albedos of Haut Glacier d'Arolla, Switzerland. *Int. J. Remote Sens.*, in press.

Knowles Middleton, W. E., and Mungall, A. G. (1952), The luminous directional reflectance of snow. *J. Opt. Soc. Am.* 43:572–579.

Kuhn, M. (1985), Bidirectional reflectance of polar and Alpine snow surfaces. *Ann. Glaciol.* 6:164–167.

Lindsay, R. W., and Rothrock, D. A. (1994), Arctic sea ice albedo from AVHRR. *J. Clim.* 7:1737–1749.

Markham, B. L., and Barker, J. L. (1983), Spectral characterization of the Landsat Thematic Mapper sensors. In *Proceedings of the Landsat-4 Science Characterization Early Results Symposium*, NASA Conference Publication 2355, February, pp. 235–276.

Oerlemans, J. (1997), Glacio-meteorlogical investigations on the Morteratschgletscher, Switzerland, Report No. 1, Summary of 1 October 1995–1 October 1996. Internal Publication IMAU R 97-7, Utrecht University, Utrecht, The Netherlands.

Oerlemans, J., and Knap, W. H. (1998), A one-year record of global radiation and albedo in the ablation zone of the Morteratschgletscher, Switzerland. *J. Glaciol.*, in press.

Salomonson, V. V., and Marlatt, W. E. (1968), Anisotropic solar reflectance over white sand, snow and stratus clouds. *J. Appl. Meteorol.* 7:475–483.

Slingo, A., and Schrecker, H. M. (1982), On the shortwave radiative properties of stratiform water clouds. *Quart. J. Roy. Meteorol. Soc.* 108:407–426.

Steffen, K. (1987), Bidirectional reflectance of snow at 500–600 nm. In *Large Scale Effects of Seasonal Snow Cover, Proceedings of the Vancouver Symposium*, August, IAHS Publ. No. 166, pp. 415–425.

Suttles, J. T., Green, R. N., Minnis, P., et al. (1988), *Angular Radiation Models for Earth–Atmosphere System. Volume I: Shortwave Radiation*, NASA Reference Publication 1184, NASA, Washington, DC.

Taylor, V. R., and Stowe, L. L. (1984), Reflectance characteristics of uniform earth and cloud surfaces derived from NIMBUS-7 ERB. *J. Geophys. Res.* 89(D4):4987–4996.

Walthall, C. L., Norman, J. M., Welles, J. M., Campbell, G., and Blad, B. L. (1985), Simple equation to approximate the bidirectional reflectance from vegetative canopies and bare soil surfaces. *Appl. Opt.* 24(3):383–387.

Warren, S. G. (1982), Optical properties of snow. *Rev. Geophys. Space Phys.* 20(1):67–89.

Winther, J.-G. (1993), Landsat TM derived and in situ summer reflectance of glaciers in Svalbard. *Polar Res.* 12(1):37–55.

Winther, J.-G. (1994), Spectral bi-directional reflectance of snow and glacier ice measured in Dronning Maud Land, Antarctica. *Ann. Glaciol.* 20:1–5.

Wiscombe, W. J., and Warren, S. G. (1980), A model for the spectral albedo of snow: pure snow. *J. Atmos. Sci.* 37(12):2712–2733.